

Article

# The Use of Co-Precipitation to Produce Nano-Mn–Zn Ferrite ( $[\text{Mn}_x\text{Zn}_{1-x}]\text{Fe}_2\text{O}_4$ ) from Waste Batteries

Yenchun Liu \* and Jarnchih Hsu

Graduate School of OptoMechatronics and Materials, WuFeng University, Chiayi 62153, Taiwan;  
billy88094266@gmail.com

\* Correspondence: bliu@wfu.edu.tw; Tel.: +886-953-303683; Fax: +886-5-206-3264

Received: 25 April 2018; Accepted: 16 June 2018; Published: 20 June 2018



**Abstract:** This study uses pure materials or waste batteries to produce a nanoscale Mn–Zn ferrite. Acid is used to dissolve the battery into solution and then co-precipitation is used to produce nanoscale ferrite. When the calcination temperature in an air atmosphere exceeds 600 °C,  $\alpha\text{-Fe}_2\text{O}_3$  is generated and there is a decrease in the saturated magnetization. Using waste batteries to produce  $[\text{Mn}_{0.54}\text{Zn}_{0.46}]\text{Fe}_2\text{O}_4$  at a pH of 10, the saturated magnetization is 62.85 M (emu/g), which is optimal. At a pH of 10, the particulate diameter is largest, at about 40 nm. The stronger the crystal phase of Mn–Zn ferrite, the greater is the saturated magnetization. The ferrite crystal phase is analyzed using X-ray diffraction (XRD), scanning electron microscopy (SEM) and a vibrating sample magnetometer (VSM). The stronger the crystal phase, the larger is the average particulate diameter. The magnetic properties, the particulate diameter and the magnetic flux density of ferrite powders that are prepared under different conditions are studied.  $[\text{Mn}_x\text{Zn}_{1-x}]\text{Fe}_2\text{O}_4$  ferrite powders can be used as an iron core and as resonance imaging materials.

**Keywords:** co-precipitation method; ferrite; saturated magnetization

## 1. Introduction

Ferrite cores are a vital inductive component in motors for computer, communication and consumer Electronics (3C) products, so they are an important raw material for the industry. Traditional production methods use  $\text{MnO}_2$ ,  $\text{ZnO}$  and  $\text{Fe}_2\text{O}_3$  as raw materials, and a solid-state reaction is initiated. When the raw materials are mixed, sintered and ground, a powder is produced. This powder is granulated, formed and placed in a nitrogen furnace for sintering, before it is made into an iron core. If waste batteries are used as the raw material, this cost is reduced and the process is environmentally friendly. Dry batteries can only be used once and are then discarded, which is a waste of a resource and material and pollutes the environment because the batteries contain Hg. In this study, waste batteries are used as the raw material and co-precipitation is used to prepare Zn–Mn series ferrite. The magnetic properties, the particulate diameter and the magnetic flux density of both types of ferrite core are studied.

The manufacture of ferrite involves forming and sintering an inorganic material (which does not contain carbon–hydrogen compounds) using a process that is the same as that for the production of ceramics. Ferrites are the earliest forms of fine ceramic [1,2]. Ferrite structures are classified into three main categories [3,4]: (1) spinel structure, such as the Zn–Mn series and the Ni–Zn series, which exhibits ferromagnetism and good permeability ( $i_i$ ), magnetic flux density ( $B_s$ ) and loss characteristics; (2) garnet structure, such as yttrium iron oxide, which exhibits anti-ferromagnetism and is mainly used in microwave communication and laser optics applications; and (3) hexagonal structure, such as ferrites of the Ba series and Sr series, which exhibits permanent magnetism and is also called hard ferrite. The preparation methods for ferrite include: (1) the solid-state reaction method,

for which metallic oxide powder is used as the raw material and the raw materials are mixed, sintered and ground to produce ferrite powder [5–7]; (2) the co-precipitation method, for which metallic ion salt is used as the raw material and dissolved, mixed, neutralized by adding alkali, oxidized by aeration, rinsed with water, and baked and ground to produce ferrite powder [8–10], and then after high-temperature sintering, ferrite powder is produced; (3) the sol–gel process, for which metallic ion salt is used as the raw material and citric acid is added, whereupon the mixture is agitated and finally undergoes vacuum rotary evaporation to produce a viscous liquid [11–14]; and (4) the hydrothermal method, which uses a pressurized solution at a temperature that is greater than the normal boiling point of water or the solvent in an autoclave. Because of the high temperature and high pressure, the solubility, the diffusion coefficient and the reactivity of the solute are significantly increased and the reaction is easier to initiate [15–17]. In 2017, Quin reported precise control the  $\text{Fe}^{2+}$  concentration, pH, temperature and aeration rate to synthesise, with size of 10–300 nm, cube-like and sphere-like crystalline  $\text{Fe}_3\text{O}_4$  nanoparticles [18].

In a primary battery, the positive electrode of a Zn–Mn dry battery is  $\text{MnO}_2$ , and the negative electrode is Zn. The electrolyte between the positive and negative electrodes is  $\text{ZnCl}_2$  or  $\text{NH}_4\text{Cl}$ . In an alkaline Mn battery, the positive electrode is also  $\text{MnO}_2$  and the negative electrode is Zn, but the electrolyte between the positive and negative electrodes is KOH. The only difference between these two batteries is the electrolyte that is used. Therefore, waste batteries can be used as a raw material to produce of Zn–Mn ferrite. The recovery of Mn from Zn–Mn and Zn–C battery waste has been the subject of studies [19–22]. In this experiment, co-precipitation at different pH values (pH of 6–12) and different sintering temperatures (0–1200 °C) is used to synthesize  $[\text{Mn}_x\text{Zn}_{1-x}]\text{Fe}_2\text{O}_4$  nano-ferrite powder. The effect of the pH value on the strength and integrity of the crystal phase is determined, and the effect of the sintering temperature on the saturated magnetization ( $M_s$ ), the remanant magnetization ( $M_r$ ), the coercive force ( $H_c$ ), the magnetic flux ( $B$ ) and the average particulate diameter ( $D$ ) is measured. Mn–Zn ferrites are prepared under different conditions and the differences in the physical properties and electromagnetic properties of the nano-powders that are produced using pure material and waste batteries are determined.

## 2. Experimental

### 2.1. Materials and Measurement Tools

Sulfuric acid ( $\text{H}_2\text{SO}_4$ ), hydrochloric acid (HCl), sodium hydroxide (NaOH), zinc (II) nitrate ( $\text{Zn}(\text{NO}_3)_2 \cdot 6\text{H}_2\text{O}$ ), ferric (III) nitrate ( $\text{Fe}(\text{NO}_3)_3 \cdot 9\text{H}_2\text{O}$ ), manganese nitrate, ( $\text{Mn}(\text{NO}_3)_2 \cdot 6\text{H}_2\text{O}$ ), nickel nitrate ( $\text{Ni}(\text{NO}_3)_2 \cdot 6\text{H}_2\text{O}$ ) and other reagents that were used for synthesis were all G.R.-grade chemicals. A computer-interface X-ray powder diffractometer (XRD) that uses Cu  $K\alpha$  radiation (Multiflex, Rigaku, Tokyo, Japan) was used to identify the nanoparticles. The morphology of particles was determined using a scanning electron microscope (SEM, Hitachi S3000N, Tokyo, Japan) with an accelerating voltage of 15 kV. A field-emission scanning electron microscope (FESEM, JEOL, JSM-6700F, Tokyo, Japan) was used to characterize the surface structure of the nanoparticles. A vibrating sample magnetometer (VSM, ADE-DMS Model 1660, MA, USA) was used to observe the electromagnetic properties of the nanoparticles. An oxygen analyzer measured the oxygen concentration (Chang-Ai, CI1000, Shanghai, China). Composite particles of ferrite were produced by sintering in a high-temperature furnace (AcuTech systems Co., Ltd. BAT-750, New Taipei, Taiwan).

### 2.2. The Use of Waste Dry Batteries to Produce Nano-Mn–Zn Ferrite ( $[\text{Mn}_x\text{Zn}_{1-x}]\text{Fe}_2\text{O}_4$ )

The dry battery was crushed and dissolved using steel acid cleaning waste solution and then heated to 70–80 °C to accelerate the dissolution process. Filter paper was then used to filter the dissolved solution, in order to remove the spacer material, the pulp and the plastic pad in the battery. The filtered solution and waste iron powder were then used for a displacement reaction at a temperature of about 35 °C. This reaction displaces Cu, Cd, Pb and Hg in ionic solution. Filter paper

was then used to filter out the displaced metal and alkali was added to the filtered solution to neutralize it to a pH of 9. An air pump was used to pass air over the sample at a temperature of 80 °C, to allow oxidation for 24 h. Filter paper was then used to filter out the ferrite powder containing salt. Distilled water was used to remove the salt from the filter cake. This operation was repeated 5 to 6 times, to completely remove the salt. The residue was placed in a baking oven to bake dry at 120 °C and the resultant product was ground using an agate mortar. The sample was heated to 600 °C and 10% of PVA was used for granulation. The product was then placed in a mold and pressed into a tablet. Nitrogen gas was then used to sinter it at a high temperature, to produce a ferrite core. The flow chart for the process is shown in Figure 1.

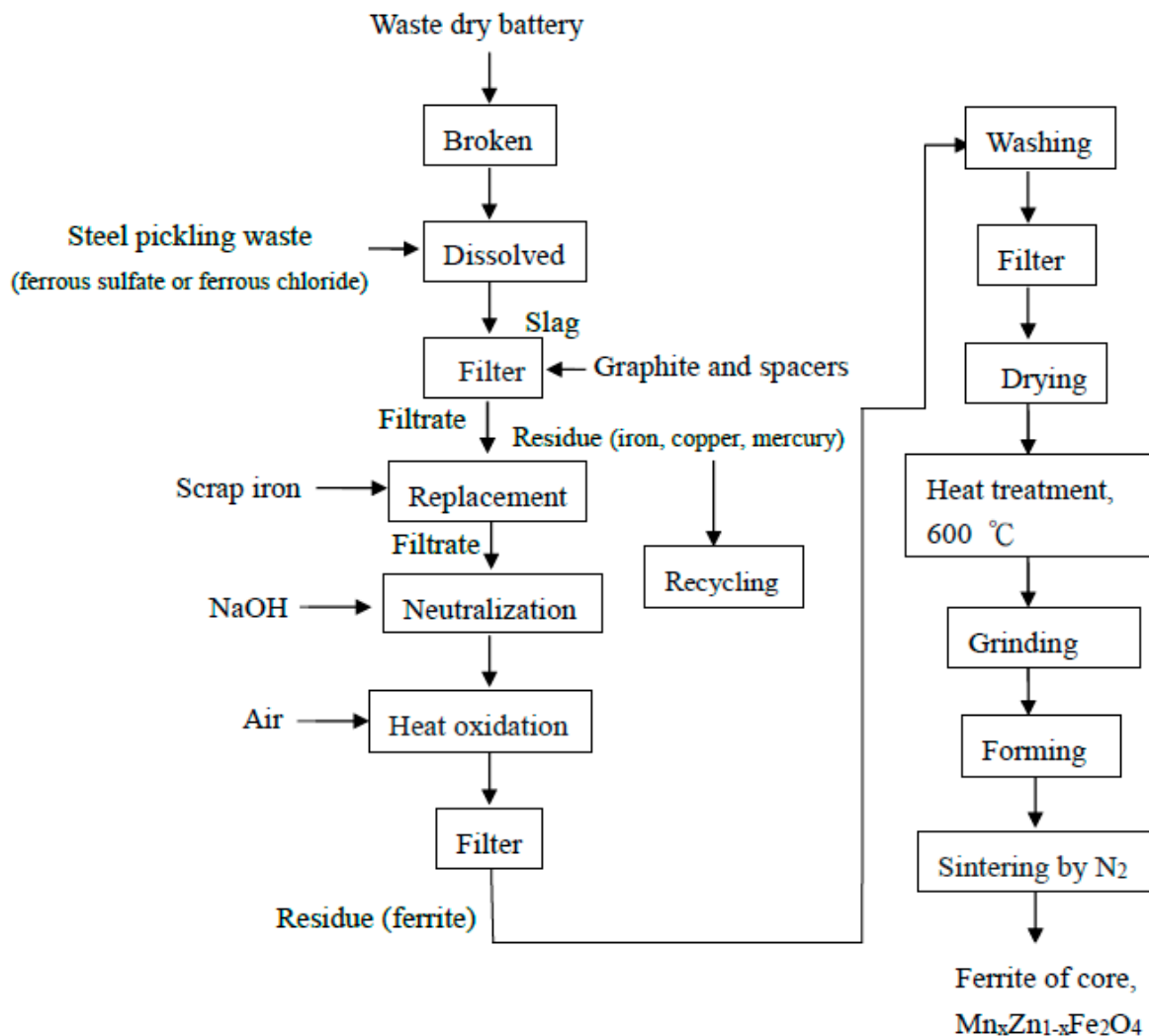
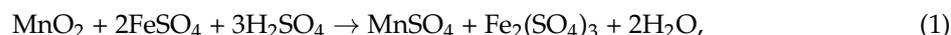


Figure 1. The synthesis of  $[\text{Mn}_x\text{Zn}_{1-x}]\text{Fe}_2\text{O}_4$  ferrite from waste battery.

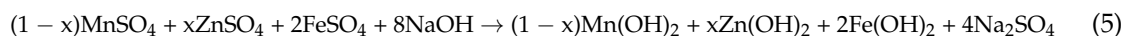
### 2.3. The Chemical Reaction Mechanism and an Analysis of the Use of a Dry Battery to Prepare Ferrite

Waste batteries were used as the raw material to produce Mn–Zn ferrite. The waste batteries and the waste solution form a metallic ion solution, which is neutralized and precipitated using NaOH. After passing through air to allow oxidation and to remove the salt, the product is sintered at a high temperature to produce  $[\text{Mn}_x\text{Zn}_{1-x}]\text{Fe}_2\text{O}_4$  ferrite.  $\text{MnO}_2$  in the dry battery and ferrous sulfate and sulfuric acid in the steel acid cleaning waste solution react to form  $\text{MnSO}_4$ ,  $\text{FeSO}_4$  and water. Fe in dry the battery reacts with the  $\text{FeSO}_4$  that is dissolved in steel acid cleaning waste solution to form ferrous sulfate, and then forms ferric sulfate and hydrogen. Zn in the dry battery reacts with

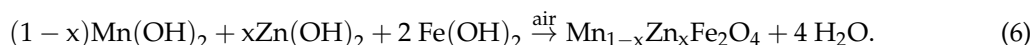
sulfuric acid in the steel acid cleaning waste solution to form  $\text{ZnSO}_4$  and hydrogen. Finally, Hg in the dry battery reacts with ferrous sulfate in the steel acid cleaning waste solution to form  $\text{HgSO}_4$  and ferric sulfate. The formulae for these reactions are:



When the dry battery is dissolved in steel acid cleaning waste solution, four metallic ion solutions that contain sulfate are obtained. Waste iron powder is added into  $\text{HgSO}_4$  to displace Hg, and three metallic ion solutions of Mn, Zn and Fe are formed. Based on the stoichiometric ratio, one mole of  $\text{MnO}_2$ , Fe and Zn requires a total of five moles of acid to dissolve completely. It is generally ensured that the reaction is complete by adding excess acid. NaOH is added to neutralize the sulfate, and the product was precipitated to yield hydroxide.



Air is passed over the metal hydroxide to oxidize it and to produce  $\text{Mn}_{1-x}\text{Zn}_x\text{Fe}_2\text{O}_4$ . The reaction formula is



An inductively coupled plasma (ICP) was used to measure the metal ion content in the battery solution. There was a large excess of Fe ions so the solution was supplemented with Mn and Zn. The solution was adjusted according to that was required for different Mn–Zn compositions. The entire reaction uses a waste battery and steel acid cleaning waste solution as raw materials, and the battery is dissolved into ionic solution. After the displacement reaction, impurities such as Cu, Hg and Cd in ionic solution are removed and NaOH solution is used to precipitate the metallic ion. Air is passed over the product and heat is introduced to oxidize the metallic solution that carries the OH root, which slowly forms into ferrite with a spinel structure. The recovery rate of useful materials for waste batteries was 83.92 wt %. This method can save the cost of  $\text{MnO}_2$ , Fe, Zn and Fe raw materials, and solve the problem of waste batteries and waste acid pollution.

### 3. Results and Discussions

#### 3.1. The Effect of Different Mn and Zn Contents on the Crystal Phase

Figure 2a shows the XRD diffractogram of  $[\text{Mn}_x\text{Zn}_{1-x}]\text{Fe}_2\text{O}_4$  for different proportions of Mn and Zn. The diffraction peak shows that a change in the proportions affects the crystal phase. The crystal phase for a composition of  $\text{Mn}_{0.54}\text{Zn}_{0.46}\text{Fe}_2\text{O}_4$  is the most integrated and the strongest. The crystal phase for  $\text{Mn}_{0.8}\text{Zn}_{0.2}\text{Fe}_2\text{O}_4$  is the least integrated and the weakest. The nano-Mn–Zn ferrite ( $[\text{Mn}_x\text{Zn}_{1-x}]\text{Fe}_2\text{O}_4$ ) is a spinel structure. The average particulate diameter is calculated using the diffraction peaks for different Mn–Zn proportions and the Scherrer equation. It is seen that the particulate diameter is different for different crystal phases. For the composition  $[\text{Mn}_{0.54}\text{Zn}_{0.46}]\text{Fe}_2\text{O}_4$  with the strongest crystal phase, the largest average particulate diameter is 11.50 nm. For the composition  $[\text{Mn}_{0.8}\text{Zn}_{0.2}]\text{Fe}_2\text{O}_4$  with the weakest crystal phase, the average particulate diameter is the smallest, at about 4.28 nm.

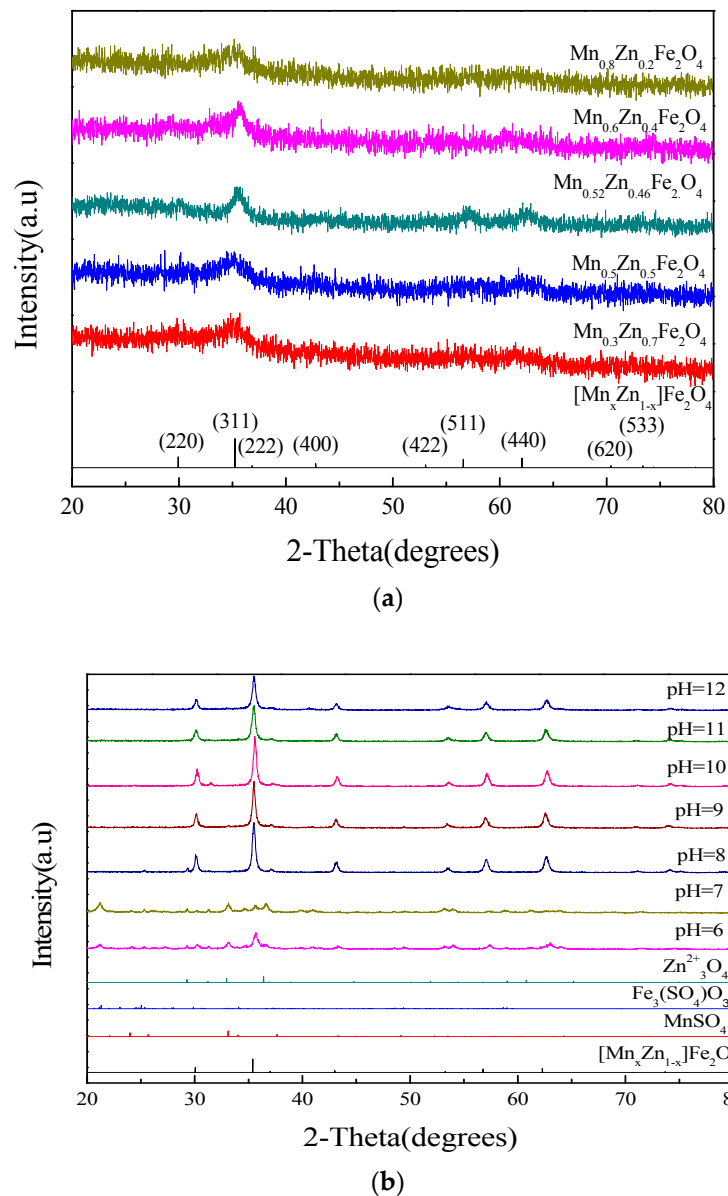


**Figure 2.** XRD patterns for (a)  $[\text{Mn}_x\text{Zn}_{1-x}]\text{Fe}_2\text{O}_4$  sintered at  $600\text{ }^\circ\text{C}$  and (b) the effect of the pH value of the waste dry battery.

Figure 2b shows the effect of the pH value of the waste battery on the crystal phase of  $[\text{Mn}_x\text{Zn}_{1-x}]\text{Fe}_2\text{O}_4$ . It is seen that for pH values between 6 and 7, there are many phases in the diffraction peaks. For a pH value of 8, the strength of the crystal lattice of the miscellaneous phase is greatly reduced. For a pH value of 10, the diffraction peak for the miscellaneous phase is totally absent. The miscellaneous peak is the diffraction peak for  $\text{Zn}^{2+}_3\text{O}_4$ ,  $\text{Fe}_3(\text{SO}_4)_3\text{O}_3$  and  $\text{MnSO}_4$ , and when the pH value is between 6 and 7, there is insufficient alkaline content so the Fe ions and Mn ions are not fully precipitated, and the precipitated  $\text{Zn}^{2+}_3\text{O}_4$  forms Zn ions. The solution must be neutralized to a pH value of greater than 9.

The average particulate diameter for  $[\text{Mn}_x\text{Zn}_{1-x}]\text{Fe}_2\text{O}_4$  at different pH values is calculated using the diffraction peak and the Scherrer equation. Normally, crystallite size decreases as the particle size decreases, but not at the same rate. Nitrogen adsorption (BET) is a good technique for measuring nano-ferrite particles [23]. A pH value of 6 produces the smallest average particulate diameter of about 31.10 nm because the alkaline content is not sufficient and the sulfate in the ionic solution is

not neutralized, so the metallic ions are not precipitated and a complete spinel structure cannot grow. For higher pH values, the average particulate diameter is greater. A pH value of 10 gives the maximum average particulate diameter of about 59.61 nm. Further increases in the pH value result in a decrease in the average particulate diameter because when the pH value is too large,  $\text{Zn}(\text{OH})_2$  reacts with NaOH to form  $\text{Na}_2\text{ZnO}_2$  and the Zn atoms in the spinel structure are removed. A pH value of 12 gives an average particulate diameter of only 35.03 nm. The particulate diameter varies between 31.10 and 59.61 nm for the range of pH values that is used in this study.

### 3.2. The Effect of Different Mn and Zn Contents on the Magnetic Properties

For a composition  $\text{Mn}_{0.54}\text{Zn}_{0.46}\text{Fe}_2\text{O}_4$ , the saturated magnetization is about 0.01 M (emu/g) more than that for  $\text{Mn}_{0.5}\text{Zn}_{0.5}\text{Fe}_2\text{O}_4$ , so the composition  $\text{Mn}_{0.54}\text{Zn}_{0.46}\text{Fe}_2\text{O}_4$  is used to determine the effect of sintering temperature on Mn–Zn ferrite. The hysteresis curves (pH of 9, 80 °C, air oxidation for 24 h) for ferrites with different compositions of Mn–Zn, Ni–Zn and Cu–Zn at the same pH value are shown. We show that the saturated magnetization for a  $[\text{Mn}_x\text{Zn}_{1-x}]\text{Fe}_2\text{O}_4$  system that is recycled from waste batteries is at a maximum. For ferrites of Mn–Zn, Ni–Zn and Cu–Zn, when the pH is 9, the results show that the value for the coercive force ( $H_c$ ) does not exceed 200 Oersted (Oe) and the  $M_r$  value approaches zero (soft ferrite has a lower remanent magnetization), which demonstrates that the ferrites for all of the systems are soft ferrites, as shown in Figure 3.

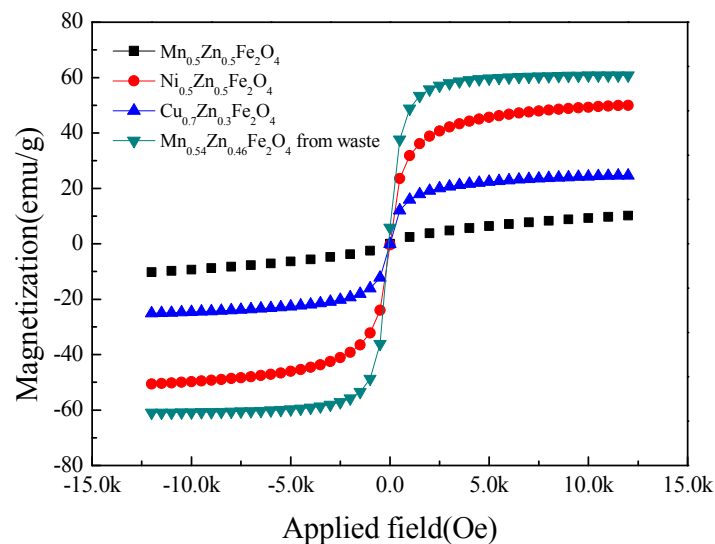


**Figure 3.** The hysteresis curves for different compositions and proportions;  $[\text{M}_x\text{Zn}_{1-x}]\text{Fe}_2\text{O}_4$  ( $M = \text{Mn}, \text{Zn}, \text{Cu}$ ).

### 3.3. The Effect of the pH Value on the Magnetic Properties of $[\text{Mn}_{0.54}\text{Zn}_{0.46}]\text{Fe}_2\text{O}_4$

Figure 4 shows the effect of coercive force ( $H_c$ ) on the saturated magnetization ( $M_s$ ) and the remanent magnetization ( $M_r$ ) for  $[\text{Mn}_{0.54}\text{Zn}_{0.46}]\text{Fe}_2\text{O}_4$  at different pH values. It is seen that the  $H_c$  value does not exceed 200 Oe and that the  $M_r$  value (soft ferrite has a lower remanent magnetization) approaches zero. This demonstrates that this series is soft ferrite. In terms of the effect of the pH value of the waste battery on the magnetic properties of Mn–Zn ferrite, it is seen that the saturated magnetization has the lowest value of 2.52 M (emu/g) for a pH value of 6, because metallic ions do not precipitate completely so a complete structure is not formed. The spinel structure at a pH value of 10 has a lower saturated magnetization. The peak value for the saturated magnetization is 62.85 M (emu/g), and the crystal phase is the most complete. The saturated magnetization decreases when the pH value is 11, because an increase in the pH value inhibits the precipitation of Zn ions. For a pH value of 12, the saturated magnetization is only 44.81 M (emu/g). The coercive force ( $H_c$ ), the saturated magnetization

(Ms) and the remanent magnetization (Mr) for a composition of MnZnFe<sub>2</sub>O<sub>4</sub> at different pH values are shown in Table 1. The data shows that, for the different pH values, the magnetic properties and the value of Hc do not exceed 200 Oe. The value for Mr is also quite low, which demonstrates that this series is soft ferrite. The magnetic flux (B) for [Mn<sub>0.54</sub>Zn<sub>0.46</sub>]Fe<sub>2</sub>O<sub>4</sub> at different pH values is calculated in gauss. The magnetic flux at a pH of 6 is 102.95 gauss/g. An increase in the pH value produces a corresponding increase in magnetic flux. At a pH of 10, the peak value is 864.48 gauss/g. This value decreases to 637.78 gauss/g for a pH of 12. The magnetic flux (B) for [Mn<sub>0.54</sub>Zn<sub>0.46</sub>]Fe<sub>2</sub>O<sub>4</sub> increases from 102.95 (gauss/g) at a pH value of 6 to a peak value of 864.48 (gauss/g) at a pH value of 10. At pH values of greater than 10, the value begins to decrease because Zn ions do not precipitate completely. The pH was changed from 6 to 12, the particle size was changed from 31 to 59 nm, Ms was changed from 2.52 to 62.85 emu/g. The Mn–Zn ferrite nanoparticles’ size and structure (cube-like NPs or sphere-like NPs) affects the NPs’ magnetic properties. Smaller NPs have more defects, and a decrease of  $\mu$  and Ms properties. This is consistent with a previous study on the particle size and magnetic properties [18].

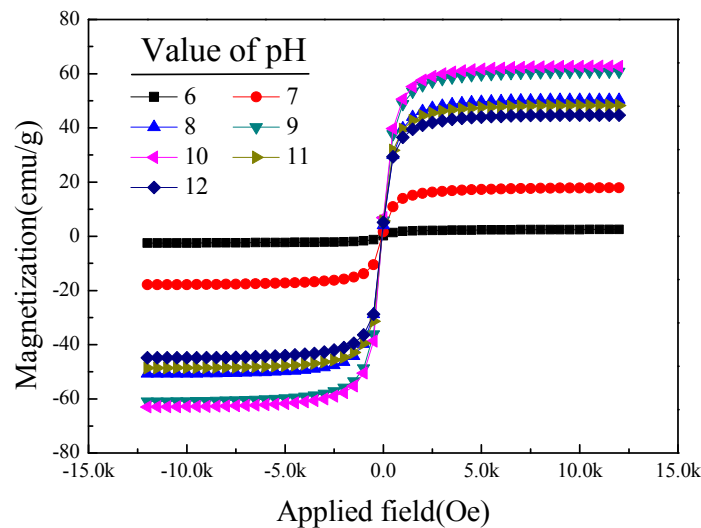


**Figure 4.** The effect of the pH value on the magnetic properties of [Mn<sub>0.54</sub>Zn<sub>0.46</sub>]Fe<sub>2</sub>O<sub>4</sub> that is produced from waste dry batteries.

**Table 1.** The effect of various factors on the magnetic properties of [Mn<sub>0.54</sub>Zn<sub>0.46</sub>]Fe<sub>2</sub>O<sub>4</sub> that is produced from waste dry batteries.

Condition	Property	Hc(Oe)	Ms (emu/g)	Mr (emu/g)	B (gauss/g)
pH	6	71.30	2.52	0.20	102.95
	7	65.81	17.90	1.59	290.63
	8	61.65	50.56	4.05	696.68
	9	69.53	60.89	5.83	834.31
	10	75.08	62.85	6.84	864.48
	11	76.43	48.45	5.68	684.96
	12	74.97	44.81	5.08	637.78
Temperature (°C) by air	500	34.61	4.96	0.03	96.91
	600	2.71	16.64	0.01	211.71
	700	11.45	9.97	0.02	136.67
	800	46.29	2.57	0.02	78.57
Temperature (°C) by N <sub>2</sub> gas	700	17.36	16.32	0.29	222.34
	800	16.84	42.36	0.81	548.88
	900	22.54	36.58	1.06	481.98
	950	32.97	33.86	1.51	458.25

### 3.4. The Effect of Sintering Temperature on the Crystal Phase and the Magnetic Properties

Figure 5a shows the XRD diagram (sintering in an air atmosphere, an increase in temperature of 5 °C/min, and then a constant temperature for 2 h, followed by cooling in a furnace) for  $[\text{Mn}_{0.54}\text{Zn}_{0.46}]\text{Fe}_2\text{O}_4$  that is sintered at different temperatures. It is seen that when the sintering temperature is increased, the XRD diffraction peak increases in height, so the strength of the ferrite increases. An increase in the sintering temperature produces particle with a greater diameter. When the calcination temperature is 700 °C, the XRD diffraction peak shows slight amounts of  $\alpha\text{-Fe}_2\text{O}_3$ . When the sintering temperature is increased to 800 °C, the diffraction peak for  $\alpha\text{-Fe}_2\text{O}_3$  is larger. This demonstrates that in an air atmosphere, when the sintering temperature exceeds 600 °C,  $\alpha\text{-Fe}_2\text{O}_3$  is generated immediately and there is a decrease in the saturated magnetization for Mn–Zn ferrite. The value for the average particulate diameter for  $[\text{Mn}_{0.54}\text{Zn}_{0.46}]\text{Fe}_2\text{O}_4$  that is sintered in an air atmosphere at different temperatures is calculated using the diffraction peak. The value is 11.50 nm for unsintered material, and an increase in the sintering temperature produces an increase in the average particulate diameter. At temperatures greater than 600 °C, decomposition occurs because Mn is oxidized. However, the average particulate diameter for  $\alpha\text{-Fe}_2\text{O}_3$  increases when the sintering temperature is increased, so even if there is decomposition because Mn is oxidized, the average particulate diameter increases until the sintering temperature is 800 °C, at which temperature the average particulate diameter is 69.20 nm.

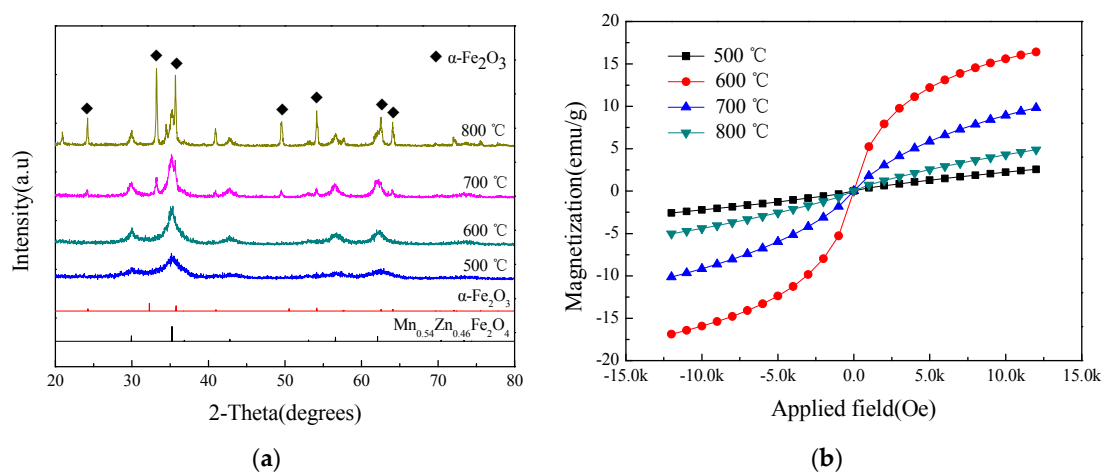


**Figure 5.** The effect of the sintering temperature in an air atmosphere on (a) the crystal phase and (b) the magnetic properties.

Figure 5b shows the effect of sintering temperature on the magnetic properties, using the hysteresis curve for  $[\text{Mn}_{0.54}\text{Zn}_{0.46}]\text{Fe}_2\text{O}_4$  at different sintering temperatures. A sintering temperature of 600 °C results in the greatest value for saturated magnetization. When the sintering temperature exceeds 600 °C, the saturated magnetization begins to decrease. A sintering temperature of 800 °C gives a saturated magnetization of 2.57 M (emu/g), which is less than the value for unsintered ferrite. When the temperature is increased, there is an increase in thermal vibration in the lattice. The binding energy for the oxygen atoms also decreases, so these escape [2]. When the sintering temperature exceeds 600 °C, the amount of  $\alpha\text{-Fe}_2\text{O}_3$  in the crystal phase is increased ( $\alpha\text{-Fe}_2\text{O}_3$  is also called hematite, which is not magnetic [24,25]). If sintering is performed in a  $\text{N}_2$  atmosphere, a reducing environment is formed within the furnace.

The results for the magnetic flux for  $[\text{Mn}_{0.54}\text{Zn}_{0.46}]\text{Fe}_2\text{O}_4$  at different sintering temperatures show that the magnetic flux at a temperature of 500 °C is 96.91 gauss/g. An increase in the sintering temperature produces an increase in the magnetic flux. When the temperature is 600 °C, there is a maximum value of about 211.71 gauss/g and the value then begins to decrease for higher temperatures,

because when sintering is performed in an air atmosphere, the Fe atoms in  $[\text{Mn}_x\text{Zn}_{1-x}]\text{Fe}_2\text{O}_4$  are thermally disassociated into  $\alpha\text{-Fe}_2\text{O}_3$ .

### 3.5. Surface Morphology and Compositional Analysis of $[\text{Mn}_{0.54}\text{Zn}_{0.46}]\text{Fe}_2\text{O}_4$

Figure 6 shows the surface morphology for  $[\text{Mn}_{0.54}\text{Zn}_{0.46}]\text{Fe}_2\text{O}_4$  that is produced from waste batteries with different pH values. For all compositions, the Mn–Zn ferrites show similar morphology and very strong agglomeration due to magnetic particles, and particles that are of uniform grain size. It is seen that when the pH value is 6, the average particulate diameter is very small, at about 10 nm. There is a laminate structure, when the pH value is 7, but the average particulate diameter remains at about 10 nm. The laminate structure decays when the pH has a value of 8 because the particles begin to cluster into ball shapes. The laminate structure almost disappears when the pH is 9 and totally disappears at a pH of 10, when only nanoparticles that are clustered into spherical shapes remain. The average particulate diameter increases significantly to about 40 nm and there is no laminate structure when the pH value is 11. It is seen that for a pH value of 12, the average particulate diameter is smaller than that for a pH of 10, at about 20–30 nm, and there is no laminate structure. The average particulate diameter is only about 10 nm. The laminate structure is only present at pH values of between 6 and 9, so it is reasonable to assume that the laminate structure is composed of metallic oxide that undergoes an incomplete acid or alkaline neutralization reaction.

Table 2 shows that the mean particulate diameter for  $[\text{Mn}_{0.54}\text{Zn}_{0.46}]\text{Fe}_2\text{O}_4$  is correlated with the size that is estimated from SEM and XRD using the pH value. The mean diameter for  $[\text{Mn}_{0.54}\text{Zn}_{0.46}]\text{Fe}_2\text{O}_4$  exhibits the same variation for the range of sintering temperatures studied. The energy dispersive detector (EDS) composition analysis diagram for  $[\text{Mn}_{0.54}\text{Zn}_{0.46}]\text{Fe}_2\text{O}_4$  shows that ferrite is an alloy that is formed from four elements: Mn, Zn, Fe and O. It contains no other metallic atoms. The studied proportions are correct and it is proven that the metallic ions are completely precipitated during the neutralization process.

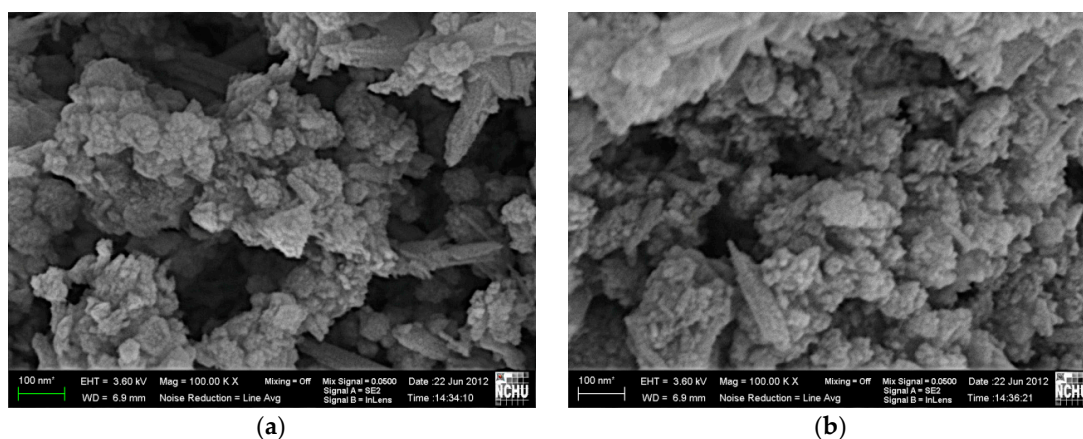
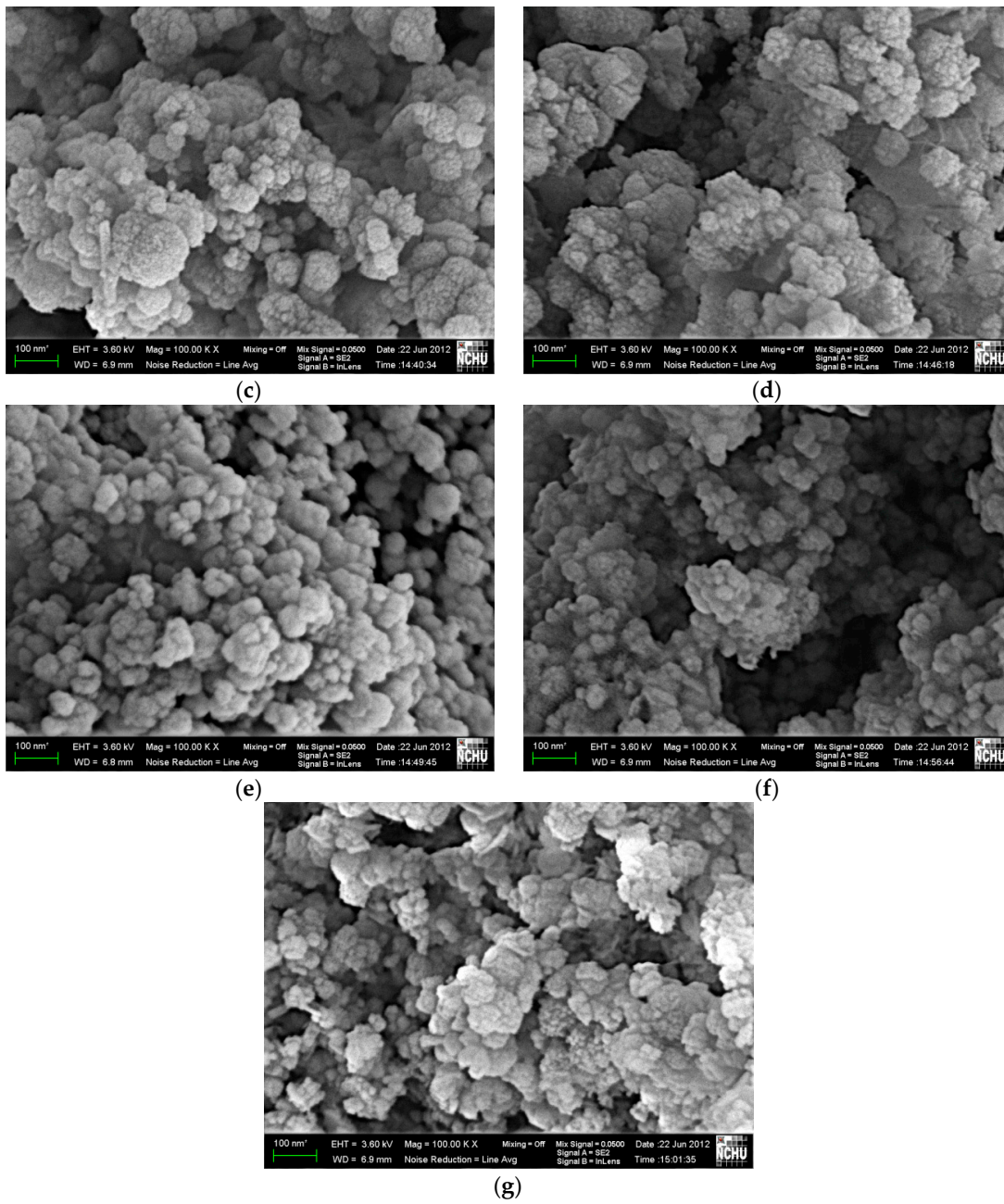


Figure 6. Cont.



**Figure 6.** The surface morphology of  $[Mn_{0.54}Zn_{0.46}]Fe_2O_4$  that is produced from waste dry batteries with different pH values: (a) pH = 6, (b) pH = 7, (c) pH = 8, (d) pH = 9, (e) pH = 10, (f) pH = 11 and (g) pH = 12.

**Table 2.** The effect of pH on the mean diameter.

pH	Composition/Method	Mn <sub>0.54</sub> Zn <sub>0.46</sub> Fe <sub>2</sub> O <sub>4</sub>	
		XRD	SEM
6		31.10	30
7		32.48	35
8		53.56	50
9		56.45	50
10		59.61	58
11		40.10	60
12		35.03	48

### 3.6. The Effect of the Sintering Temperature in a N<sub>2</sub> Environment on the Crystal Phase and the Magnetic Properties

Figure 7a shows the XRD diagram for [Mn<sub>0.54</sub>Zn<sub>0.46</sub>]Fe<sub>2</sub>O<sub>4</sub> that is sintered in a N<sub>2</sub> environment at 700 °C to 950 °C. When the ferrite is sintered at a temperature of more than 600 °C, there is oxidation, so a N<sub>2</sub> environment is used. Ferrite that is sintered in a N<sub>2</sub> environment does not contain α-Fe<sub>2</sub>O<sub>3</sub>. Table 1 shows the data for [Mn<sub>x</sub>Zn<sub>1-x</sub>]Fe<sub>2</sub>O<sub>4</sub> that is sintered at different temperatures in a N<sub>2</sub> environment. The average particulate diameter is calculated using the diffraction peaks. It is seen that when the sintering temperature is 700 °C, the particulate diameter is 95.03 nm. An increase in sintering temperature results in an increase in the average particulate diameter. At 800 °C, the value is a maximum at 119.08 nm. The value then begins to decrease and at 950 °C, it is 96.02 nm. When the material is sintered for too long in a N<sub>2</sub> environment, oxygen atoms escape from [Mn<sub>0.52</sub>Zn<sub>0.46</sub>]Fe<sub>2</sub>O<sub>4</sub>.

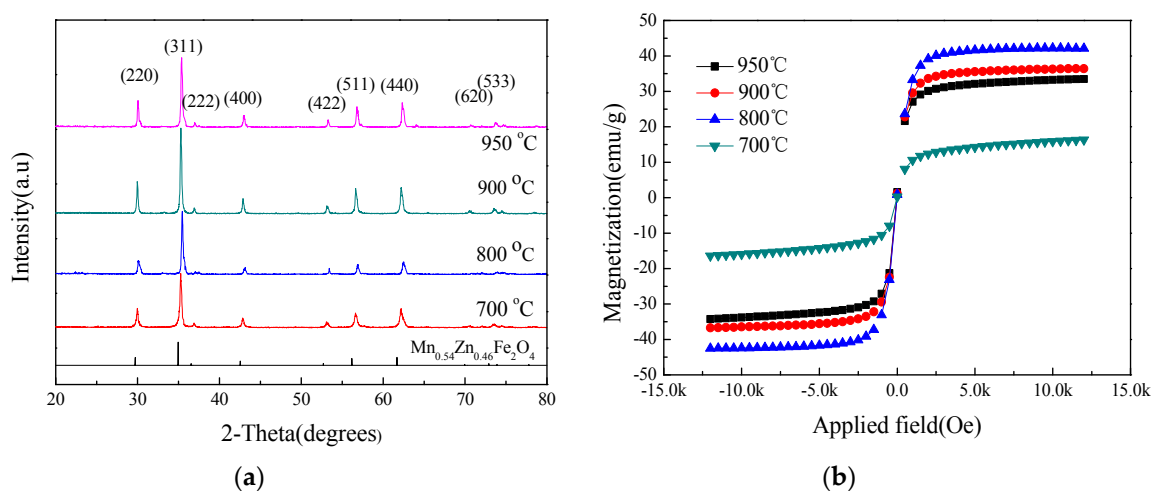


**Figure 7.** The effect of sintering temperature in a N<sub>2</sub> environment on (a) the crystal phase and (b) the magnetic properties of Mn<sub>0.54</sub>Zn<sub>0.46</sub>Fe<sub>2</sub>O<sub>4</sub>.

Figure 7b shows the hysteresis curve (sintering in a N<sub>2</sub> environment flow of 5 L/min, an increase in temperature of 5 °C/min and then maintaining a constant temperature for 2 h, followed by cooling in the furnace) that demonstrates the effect of temperature on the magnetic properties of [Mn<sub>0.52</sub>Zn<sub>0.46</sub>]Fe<sub>2</sub>O<sub>4</sub> that is sintered in N<sub>2</sub> at temperatures from 500 °C to 950 °C. It is seen that when the sintering temperature exceeds 600 °C in an air atmosphere, the saturated magnetization (M<sub>s</sub>) begins to decrease, so a N<sub>2</sub> environment was used for sintering. Figure 8b shows that for a sintering temperature of 700 °C the values are 11 M (emu/g, in an air atmosphere) and 17 M (emu/g, in a N<sub>2</sub> environment). At 800 °C, values are 2.57 and 42.36 M (emu/g). A sintering temperature of greater than 800 °C in a N<sub>2</sub> environment produces a decrease in the magnetic properties [26]. For a sintering temperature of 800 °C, the optimal duration for sintering is five hours. Iron-ore slurry is converted into

ferrite. There is a decrease in the magnetic properties because trivalent Fe in ferrite is deoxygenized to produce bivalent Fe. The results for coercive force (Hc), saturated magnetization (Ms) and remanent magnetization (Mr) for  $[\text{Mn}_x\text{Zn}_{1-x}]\text{Fe}_2\text{O}_4$  of different compositions show that the Hc value does not exceed 200 Oe and the Mr value approaches zero (soft ferrite has a lower remanent magnetization), which demonstrates that this series is soft ferrite.

Table 1 shows the magnetic flux for  $[\text{Mn}_x\text{Zn}_{1-x}]\text{Fe}_2\text{O}_4$  that is sintered in  $\text{N}_2$  at temperatures from 700 °C to 950 °C. Using the formula  $B = 4\pi \times Ms + Hc$ , the unit of magnetic flux (B) is calculated in gauss. The table shows that the magnetic flux is 222.34 gauss/g at 700 °C. The magnetic flux is 548.88 gauss/g at 800 °C. This value then begins to decrease when the temperature is increased because sintering for too long in a  $\text{N}_2$  gas results in oxygen atoms in  $[\text{Mn}_{0.54}\text{Zn}_{0.46}]\text{Fe}_2\text{O}_4$  escaping.

### 3.7. Measurement of the Electrical Properties for Forming Sintering for Different Systems

Figure 8 shows the effect of forming sintering on the Q-value for different systems. It is seen that the Q-value increases when the frequency increases. The most significant result is for recycled batteries with a composition of  $\text{Mn}_{0.34}\text{Zn}_{0.12}\text{O}(\text{Fe}_2\text{O}_3)_{0.54}$ . The next most significant result is for  $\text{Ni}_{0.5}\text{Zn}_{0.5}\text{Fe}_2\text{O}_4$ . The least significant result is for a composition of  $\text{Cu}_{0.7}\text{Zn}_{0.3}\text{Fe}_2\text{O}_4$ . For this composition, the Q-value does not increase when the frequency is greater than 70 kHz. Figure 9 shows the effect of forming sintering on the  $\mu_0$  value for different systems. The coil has an insufficient number of turns so there is a small and negative inductive value and  $\mu_0$  is negative. It is seen that the  $\mu_0$  value decreases when the frequency is increased. For recycled batteries with a composition of  $\text{Mn}_{0.34}\text{Zn}_{0.12}\text{O}(\text{Fe}_2\text{O}_3)_{0.54}$  and a composition of  $[\text{Ni}_{0.5}\text{Zn}_{0.5}]\text{Fe}_2\text{O}_4$ , the decrease is more significant. The least significant decrease occurs for a composition of  $[\text{Cu}_{0.7}\text{Zn}_{0.3}]\text{Fe}_2\text{O}_4$ . The diagram showing the effect of forming sintering on the R-value for different systems shows the resistance value of the coil, instead of the resistance value of ferrite itself. It is seen that the only composition for which the value of the resistance increases when frequency is increased is  $[\text{Ni}_{0.5}\text{Zn}_{0.5}]\text{Fe}_2\text{O}_4$ . For compositions  $[\text{Cu}_{0.7}\text{Zn}_{0.3}]\text{Fe}_2\text{O}_4$  and  $\text{Mn}_{0.34}\text{Zn}_{0.12}\text{O}(\text{Fe}_2\text{O}_3)_{0.54}$ , an increase in frequency produces an initial increase in resistance and then a decrease.

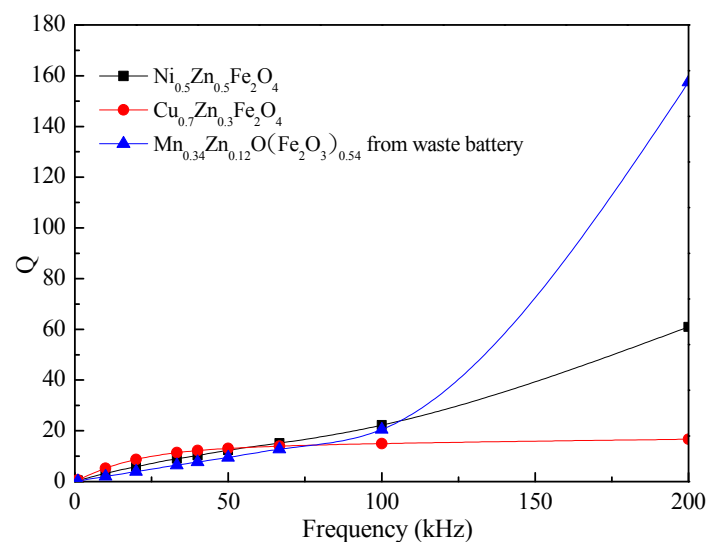


Figure 8. The effect of forming sintering on the Q-value for different systems.

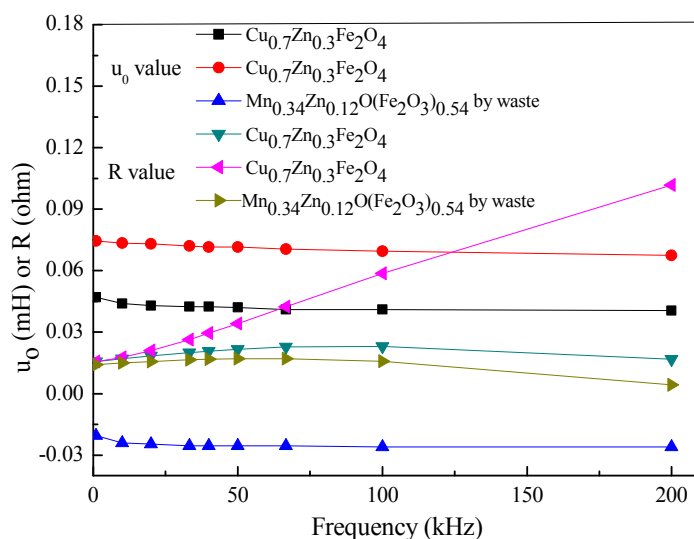


Figure 9. The effect of forming sintering on the  $\mu_0$  and R values for different systems.

#### 4. Conclusions

This study successfully produces ferrite magnets  $[\text{Mn}_{0.54}\text{Zn}_{0.46}]\text{Fe}_2\text{O}_4$  using waste batteries. When the sintering temperature exceeds  $600\text{ }^\circ\text{C}$ , Fe atoms are thermally dissociated into  $\alpha\text{-Fe}_2\text{O}_3$  and the saturated magnetization decreases. Sintering in a  $\text{N}_2$  environment increases thermal dissociation. In a  $\text{N}_2$  environment, the optimal sintering temperature is  $800\text{ }^\circ\text{C}$ , at which temperature the saturated magnetization is  $42.36\text{ M (emu/g)}$ . For sintering temperatures greater than  $800\text{ }^\circ\text{C}$ , excessively long sintering in  $\text{N}_2$  has a negative effect. The difference between the maximum and the minimum values for the saturated magnetization is  $32.14\text{ M (emu/g)}$ . These values are obtained at different sintering temperatures. The XRD diffractograms and the SEM images show that the sintering temperature affects the strength of the crystal phase. The higher the sintering temperature, the stronger is the crystal phase with a spinel structure. The average particulate diameter also increases and the higher the sintering temperature, the greater is the average particulate diameter.

The VSM images for  $\text{Mn}_x\text{Zn}_{1-x}\text{Fe}_2\text{O}_4$  with different pH values show that the optimal pH value is 9. When the pH value exceeds 9, the saturated magnetization decreases because Zn ions do not precipitate completely at higher pH values. The XRD diffractograms for different pH values for recycled batteries that are used to produce  $[\text{Mn}_x\text{Zn}_{1-x}]\text{Fe}_2\text{O}_4$  show that when the pH value is less than 9, insufficient alkaline content in the crystal phase results in incomplete precipitation of metallic ions. The VSM images show that the optimal pH value is 10. At pH values that are greater than 10, the saturated magnetization decreases because Zn ions do not precipitate completely.

The SEM images show that there is a difference between unsintered  $\text{Mn}_x\text{Zn}_{1-x}\text{Fe}_2\text{O}_4$  and  $\text{Mn}_x\text{Zn}_{1-x}\text{Fe}_2\text{O}_4$  that is sintered at  $900\text{ }^\circ\text{C}$ . The average particulate diameter is affected by sintering temperature, and varies between 10 nm and 100 nm.

**Author Contributions:** Y.L. conceived and designed the experiments; Y.L. and J.H. performed the experiments; Y.L. and J.H. analyzed the data; Y.L. contributed reagents/materials/analysis tools; Y.L. wrote the paper.

**Funding:** This research received no external funding.

**Acknowledgments:** The financial support from the Ministry of Science and Technology under grant numbers MOST 105-2221-E-274-003 and MOST 106-2221-E-274-004 is gratefully acknowledged.

**Conflicts of Interest:** The authors declare no conflict of interest. The founding sponsors had no role in the design of the study; in the collection, analyses, or interpretation of data; in the writing of the manuscript, and in the decision to publish the results.

## References

1. Smit, J.; Wijn, H.P.J. *Ferrites*; Philips Technical Library: Eindhoven, The Netherlands, 1959.
2. Murdock, E.S.; Simmons, R.F.; Davidson, R. Roadmap for 10 Gbit/in<sup>2</sup> Media: Challenges. *IEEE Trans. Magn.* **1992**, *28*, 3078–3083. [[CrossRef](#)]
3. Standley, K.J. *Oxide Magnetic Materials*, 2nd ed; Oxford University Press: Oxford, UK, 1972.
4. Ewais Emad, M.M.; Mahmoud, M.M.; Abdel-Hady, E.A. In-Situ synthesis of Magnetic Mn–Zn Ferrite ceramic object by solid state reaction. *J. Aust. Ceram. Soc.* **2008**, *44*, 57–62.
5. Topfer, J.; Angermann, A. Nanocrystalline magnetite and Mn–Zn ferrite particles via the polyol process: Synthesis and magnetic properties. *J. Mater. Chem. Phys.* **2011**, *129*, 337–342. [[CrossRef](#)]
6. Zheng, Z.G.; Zhong, X.C.; Zhang, Y.H.; Yu, H.Y. Synthesis structure and magnetic properties of nanocrystalline Zn<sub>x</sub>Mn<sub>1-x</sub>Fe<sub>2</sub>O<sub>4</sub> prepared by ball milling. *J. Alloys Compd.* **2008**, *466*, 377–382. [[CrossRef](#)]
7. Ammad, Q.H. The influence of hafnia and impurities (CaO/SiO<sub>2</sub>) on the microstructure and magnetic properties of Mn–Zn ferrites. *J. Cryst. Growth* **2006**, *286*, 365–370.
8. Upadhyay, C.; Verma, H.C.; Rath, C.; Sahu, K.K.; Anand, S.; Das, R.P.; Mishra, N.C. Mossbauer studies of nanosize Mn<sub>1-x</sub>Zn<sub>x</sub>Fe<sub>2</sub>O<sub>4</sub>. *J. Alloys Compd.* **2011**, *326*, 94–97. [[CrossRef](#)]
9. Arulmurugan, R.; Vaidyanathan, G.; Sendhilnathan, S.; Jeyadevan, B. Mn–Zn ferrite nanoparticles for ferrofluid preparation: Study on thermal-magnetic properties. *J. Magn. Magn. Mater.* **2006**, *298*, 83–94. [[CrossRef](#)]
10. Rath, C.; Sahu, K.K.; Anand, S.; Date, S.K.; Mishra, N.C.; Das, R.P. Preparation and characterization of nanosize Mn–Zn ferrite. *J. Magn. Magn. Mater.* **1999**, *202*, 77–84. [[CrossRef](#)]
11. Mane, D.R.; Patil, S.; Birajdar, D.D.; Kadam, A.B.; Shirsath, S.E.; Kadam, R.H. Sol–gel synthesis of Cr<sup>3+</sup> substituted Li<sub>0.5</sub>Fe<sub>2.5</sub>O<sub>4</sub>: cation distribution, structural and magnetic properties. *J. Mater. Chem. Phys.* **2011**, *126*, 755–760. [[CrossRef](#)]
12. Song, F.; Shen, X.; Liu, M.; Xiang, J. Preparation and magnetic properties of SrFe<sub>12</sub>O<sub>19</sub>/Ni<sub>0.5</sub>Zn<sub>0.5</sub>Fe<sub>2</sub>O<sub>4</sub> nanocomposite ferrite microfibers via sol–gel process. *J. Mater. Chem. Phys.* **2011**, *126*, 791–796. [[CrossRef](#)]
13. Klencsár, Z.; Tolnai, G.; Korecz, L.; Sajó, I.; Németh, P.; Osán, J.; Mészáros, S.; Kuzmann, E. Cation distribution and related properties of Mn<sub>x</sub>Zn<sub>1-x</sub>Fe<sub>2</sub>O<sub>4</sub> spinel nanoparticles. *Solid State Sci.* **2013**, *24*, 90–100. [[CrossRef](#)]
14. Islam, I.; Ibraheem, O.A.; Tarek, M.S.; Bahgat, A.A.; Mohamed, M.M. Synthesis of magnetically recyclable spinel ferrite (MFe<sub>2</sub>O<sub>4</sub>, M = Zn, Co, Mn) nanocrystals engineered by sol gel-hydrothermal technology: High catalytic performances for nitroarenes reduction. *Appl. Catal. B Environ.* **2016**, *181*, 389–402.
15. Lu, X.; Zhou, T.; Jia, M. Hydrothermal synthesis of Mn–Zn ferrites from spent alkaline Zn–Mn batterie. *J. Particuol.* **2009**, *7*, 491–495.
16. Saezpuche, R.; Torralvofernandez, M.J.; Gutierrez, V.B.; Gomez, R.; Marquina, V.; Marquina, M.L.; Perez Mazariego, J.L.; Ridaura, R. Ferrites nanoparticles MFe<sub>2</sub>O<sub>4</sub> (M=Ni and Zn): Hydrothermal synthesis and magnetic properties. *Boletín de la sociedad Espanola de of Cerámica y Vidrio* **2008**, *47*, 133–137.
17. Yáñez-Vilar, S.; Sánchez-Andújar, M.; Gómez-Aguirre, C.; Mira, J.M.A.; Castro-Garcia, S. A simple solvothermal synthesis of MFe<sub>2</sub>O<sub>4</sub> (M=Mn, Co and Ni) nanoparticles. *J. Solid State Chem.* **2009**, *182*, 2685–2690. [[CrossRef](#)]
18. Qing, L.; Christina, W.K.; Shinji, H.; Takashi, O.; Toru, I.; Kikuo, O. Correlation between particle size/domain structure and magnetic properties of highly crystalline Fe<sub>3</sub>O<sub>4</sub> nanoparticles. *Sci. Rep.* **2017**, *7*, 9894.
19. Cabral, M.; Pedrosa, F.; Margarido, F.; Nogueira, C.A. End-of-life Zn–MnO<sub>2</sub> batteries: Electrode materials characterization. *Environ. Technol.* **2012**, *34*, 1283–1295. [[CrossRef](#)] [[PubMed](#)]
20. Paulo, S.D.B.; Sandra, P.; Luiz, F.R.; Sequeira, C.A.C. Electrodeposition of Zn–Mn alloys from recycling Zn–MnO<sub>2</sub> batteries solutions. *Surf. Coat. Technol.* **2012**, *13*, 3036–3047.
21. Turek, A.S.; Szczepaniak, W.; Monika, Z.M. Electrochemical evaluation of manganese reducers—Recovery of Mn from Zn–Mn and Zn–C battery waste. *J. Power Sources* **2014**, *270*, 668–674. [[CrossRef](#)]
22. Sobianowska-Turek, A.; Szczepaniak, W.; Maciejewski, P.; Gawlik-Kobylińska, M. Recovery of zinc and manganese, and other metals (Fe, Cu, Ni, Co, Cd, Cr, Na, K) from Zn–MnO<sub>2</sub> and Zn–C waste batteries: Hydroxyl and carbonate co-precipitation from solution after reducing acidic leaching with use of oxalic acid. *J. Power Sources* **2016**, *325*, 220–228. [[CrossRef](#)]
23. Barba, A.; Clausell, C.; Jarque, J.C.; Monzo, M. Obtainment of nanoparticulate CuNiZn ferrite powder by high-energy milling. *J. Ceram. Soc. Jpn.* **2012**, *120*, 311–316. [[CrossRef](#)]

24. Raming, T.P.; Winnubst, A.J.A.; van Kats, C.M.; Philipse, A.P. The Synthesis and Magnetic Properties of Nanosized Hematite ( $\alpha$ -Fe<sub>2</sub>O<sub>3</sub>) Particles. *J. Colloid Interface Sci.* **2002**, *249*, 346–350. [[CrossRef](#)] [[PubMed](#)]
25. Marin, T.; Dragana, M.; Vojislav, S.; Vladan, K.; Maja, R.; Janez, P.; Zvonko, J. Synthesis and magnetic properties of concentrated  $\alpha$ -Fe<sub>2</sub>O<sub>3</sub> nanoparticles in a silica. *J. Alloys Compd.* **2007**, *441*, 291–296.
26. Gimenes, R.; Baldissera, M.R.; da Silva, M.R.A.; da Silveira, C.A.; Soares, D.A.W.; Perazolli, L.A.; da Silva, M.R.; Zaghete, M.A. Structural and magnetic characterization of Mn<sub>x</sub>Zn<sub>1-x</sub>Fe<sub>2</sub>O<sub>4</sub> ( $x = 0.2; 0.35; 0.65; 0.8; 1.0$ ) ferrites obtained by the citrate precursor method. *Ceram. Int.* **2012**, *38*, 741–746. [[CrossRef](#)]



© 2018 by the authors. Licensee MDPI, Basel, Switzerland. This article is an open access article distributed under the terms and conditions of the Creative Commons Attribution (CC BY) license (<http://creativecommons.org/licenses/by/4.0/>).